Experimental and theoretical investigation of ligand effects on the synthesis of ZnO nanoparticles

ARTICLE *in* JOURNAL OF NANOPARTICLE RESEARCH · AUGUST 2012

Impact Factor: 2.18 · DOI: 10.1007/s11051-012-1012-4

2 AUTHORS, INCLUDING:

Jin Chang
The University of Electro-Communicati…

36 PUBLICATIONS **307** CITATIONS

SEE PROFILE

J Nanopart Res (2012) 14:1012
DOI 10.1007/s11051-012-1012-4

RESEARCH PAPER

Experimental and theoretical investigation of ligand effects on the synthesis of ZnO nanoparticles

Jin Chang · Eric R. Waclawik

Received: 22 March 2012 / Accepted: 19 June 2012

Abstract ZnO nanoparticles with highly controllable particle sizes (less than 10 nm) were synthesized using organic capping ligands in $Zn(Ac)_2$ ethanolic solution. The molecular structure of the ligands was found to have significant influence on the particle size. The multi-functional molecule tris(hydroxymethyl)-aminomethane (THMA) favoured smaller particle distributions compared with ligands possessing long hydrocarbon chains that are more frequently employed. The adsorption of capping ligands on Zn_nO_n crystal nuclei (where $n = 4$ or 18 molecular clusters of (0001) ZnO surfaces) was modelled by ab initio methods at the density functional theory (DFT) level. For the molecules examined, chemisorption proceeded via the formation of Zn···O, Zn···N, or Zn···S chemical bonds between the ligands and active Zn^{2+} sites on ZnO surfaces. The DFT results indicated that THMA binds more strongly to the ZnO surface than other ligands, suggesting that this molecule is very effective at stabilizing ZnO nanoparticle surfaces. This study, therefore, provides new insight into the correlation between the molecular structure of capping ligands and the morphology of metal oxide nanostructures formed in their presence.

J. Chang · E. R. Waclawik (✉)
School of Chemistry, Physics and Mechanical Engineering, Science and Engineering Faculty, Queensland University of Technology, Brisbane, QLD 4000, Australia
e-mail: e.waclawik@qut.edu.au

Keywords Zinc oxide nanoparticles · Solvothermal synthesis · Tris(hydroxyl-methyl) aminomethane · Ab initio method · DFT simulation

Introduction

Semiconductor nanomaterials, especially low-dimensional metal oxides have attracted attention in recent years due to their size-dependent physical properties which are expected to prove to be useful in optoelectronic and other devices (Li et al. 2004; Huynh et al. 2002). Among these materials, ZnO nanostructures have been one of the most intensively studied due to their potential applications in photo-catalysis (Jian et al. 2009; Wang et al. 2009), light-emitting devices (Mao et al. 2010; Qian et al. 2011), solar cells (Westermark et al. 2002; Neubauer et al. 2011; Park et al. 2011), and gas sensors (Liao et al. 2007; Liu et al. 2011; Forleo et al. 2010; Choi and Jang 2010). For this reason, many studies have been reported on the synthesis of ZnO nanostructures by physical methods, such as by chemical vapor deposition (CVD) (Xing et al. 2006; Wu and Liu 2002), magnetron sputtering (Jouane et al. 2011), and laser ablation (Usui et al. 2004). These approaches can successfully produce high-quality nanostructures, but require special equipment or harsh conditions which hinder both their application and large scale production.

Wet chemical synthesis of ZnO nanoparticles and nanostructures for these applications has also attracted

Published online: 04 July 2012

much attention, a notable example being the innovative study of Hoffmann and coauthors (1987). Compared with physical methods, chemical synthesis holds several potential advantages, including their potential to be readily scaled-up, flexible post-synthetic processing and the fact that chemical synthesis takes place at moderate temperature (less than 200 °C). It can also be easier to isolate, purify and functionalize nanocrystals and build up nanoscale architectures through self-assembly (Shortell et al. 2010; Pacholski et al. 2002), spin-coating (Norris et al. 2003), template-assisted synthesis (Xu et al. 2010b), and similar methods (Deng et al. 2010; Mao et al. 2010). ZnO nanocrystals have been studied extensively and modified by various organic molecules, especially those with long alkyl-chains (Dev et al. 2006). For example, octanethiol has been reported to quench the growth of ZnO nanoparticles (Pesika et al. 2002). It is suggested that adsorption of thiolates on ZnO crystallite surfaces has an inhibiting effect on the crystal growth where binding of the sulfur groups to the ZnO particles results in the decrease of the particle's surface energy. Moreover, alkylamine has also been used as modifying agent in the process of ZnO synthesis. In Gamelin's study, ZnO nanocrystals were annealed in dodecylamine (DDA), which resulted in the removal or drastic deduction of defects at the ZnO surfaces leading to pure excitonic emission in the product in their fluorescence study (Norberg and Gamelin 2005). The interaction of both thiols and amines on ZnO surfaces has been investigated by X-ray photoelectron spectroscopy (XPS) (Sadik et al. 2007; Ballerini et al. 2007; Dvorak et al. 2001). Other long-chain organic ligands, such as *tert*-butyphosphonic acid (TBPA) (Cozzoli et al. 2003), octylamine (OA) (Li et al. 2004), and oleic acid (OLA) (Yin et al. 2004) have also been applied to modify ZnO nanocrystals (Luo et al. 2009). However, there are far fewer reports on the modification of ZnO nanocrystals using short-chain molecules with multifunctional groups and where these studies have been performed; the correlation between ZnO nanocrystals and ligand structures was often ignored.

In this article, we describe the synthesis of organic-modified ZnO nanoparticles (ZnO NPs) by a wet chemical method from zinc acetate solution. Tris(hydroxymethyl)aminomethane (THMA) and three other organic molecules (*n*-hexadecylamine [HDA], *n*-dodecanethiol [DDT], and *n*-trioctylphosphine oxide [TOPO]) were used as capping ligands. The ZnO samples were characterized by UV–Vis absorption, photoluminescence (PL), Fourier transform infrared (FT-IR), powder X-ray diffraction (XRD) and transmission electron microscopy (TEM). We found that these organic ligands have profoundly different effects on the growth of ZnO NPs and interparticle interactions. THMA modified ZnO NPs were produced much smaller than the particles modified by other ligands. To explain this observation, the interactions between the capping ligands and ZnO surfaces were investigated by quantum chemistry calculation based on density function theory (DFT).

Experimental

Materials

Anhydrous zinc acetate ($Zn(CH_3CO_2)_2$ or $Zn(Ac)_2$, 99.99 %), *n*-dodecanethiol ($C_{12}H_{25}SH$, or DDT, 99 %), *n*-hexadecylamine ($C_{16}H_{33}NH_2$, or HDA, 99 %), *n*-trioctylphosphine oxide ($(C_8H_{17})_3PO$ or TOPO, 99 %), tris(hydroxymethyl) aminomethane ($C_4H_{11}NO_3$ or THMA, 99 %) and absolute ethanol. All chemicals were used as received without further purification or distillation.

Synthesis of ZnO NPs

Ligand-capped ZnO NPs were synthesized by wet-chemical method. In a typical synthesis, $Zn(Ac)_2$ (0.5 mmol, 92 mg) and THMA (0.2 mmol, 24 mg) were added into absolute ethanol (30 mL) while stirring. Then the mixture was heated at around 80 °C for 1 h to dissolve $Zn(Ac)_2$ and THMA. Following complete dissolution of the precursors, a NaOH/ethanol solution (20 mL, 0.05 M) was injected into the hot solution and then refluxed for a further 72 h. The obtained cloudy solution was centrifuged and rinsed by deionized water and ethanol to remove byproducts. For the synthesis of other ligand-capped ZnO samples, all the reaction conditions were the same, except that THMA was replaced by TOPO, DDT and HDA, respectively. For comparison, bare ZnO NPs were also synthesized in the same procedure without using capping ligands.

Characterization

The absorption spectra were recorded using a Cary 100 (Varian) spectrometer. PL spectra of ZnO colloids

in ethanol were measured at room temperature with a Cary Eclipse (Varian) fluorescence spectrometer. Appropriate filters were used to avoid second-order contribution. PL spectra were taken with the absorbance of the samples at the excitation of 330 nm. FT-IR spectra were collected by a Bruker Alpha FT-IR spectrometer with attenuated total reflectance (ATR) accessory. Measurements were performed with a resolution of 4 cm^{-1} and 64 scans. XRD patterns of ZnO powders were collected with a PANalytical XPert Pro Multi Purpose Diffractometer with CuKα radiation ($\lambda = 1.54178$ Å). TEM images were obtained using a JEOL JEM-2100 microscope. The samples were prepared by dropping diluted solutions of ZnO colloids in ethanol onto 200-mesh carbon-coated copper grids and evaporating the solvent.

Computational details

ZnO in its wurzite form was created by Materials Studio software and used as the basis for the ab initio calculations (where the lattice parameters *a*, *b*, and *c* are 3.24927, 3.24927, and 5.20544 Å, respectively; and the α, β, and γ angles are 90°, 90°, and 120°, respectively; the space group of ZnO is *P*6_3*mc*). According to Nakatsuji's study (Lü et al. 1998), it is recommended that metal oxides cluster models should be cut out so as to be neutral and stoichiometric, and must contain as few dangling bonds as possible. The electronic and chemical properties (including adsorption behavior) of metal oxides are often dominated by defects such as vacancies and/or surface atoms possessing a low coordination number (Wahlström et al. 2004; Klabunde et al. 1996). Therefore, a small neutral cluster containing four Zn atoms and four O atoms (Zn_4O_4, the Z model in Fig. 1a) was used here to investigate interactions between ligands and low coordination number atoms present in a real crystal and which are likely to be highly reactive. A large cluster size was also examined in order to investigate interactions with a regular ZnO (0001) surface. This large modelled surface contained 18 Zn atoms and 18 O atoms, consisting of two layers of Zn atoms and two layers of O atoms, as shown in Fig. 1b (the ZL model). Application of these ZnO cluster sizes have been previously been used to efficiently investigate the interactions of nerve agents on ZnO surfaces (Paukku et al. 2009).

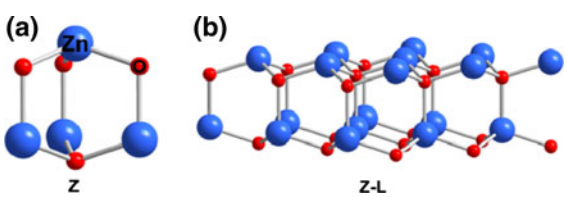

Fig. 1 Models of the ZnO surface **a** the Z (Zn_4O_4) model and **b** the Z–L ($Zn_{18}O_{18}$) model

Density functional theory (DFT) (Parr and Yang 1994) methods have been used to elucidate the interactions between ZnO surfaces and various small molecules, such as O_2 (Xu et al. 2010a), H_2O (Meyer et al. 2006), NH_3 (Martins et al. 2004), and glycine (Irrera et al. 2009). It was validated that DFT is well-suited for these weak chemical interactions on ZnO surfaces. Therefore, in our present study, calculation of adsorption of the capping ligands to the ZnO model surfaces were conducted by DFT method (Parr and Yang 1994), in conjunction with the B3LYP (Becke 1993) and LanL2DZ basis sets (Hay and Wadt 1985b; Wadt and Hay 1985; Hay and Wadt 1985a), as implemented in the Gaussian 09 program package (Frisch et al. 2009). The geometry of the THMA structure was fully optimized while the ZnO was partially or fully frozen, consistent with optimization methods used in previous studies (Martins et al. 2004; Paukku et al. 2009). The intermolecular interactions and their character were examined by the atoms in molecules (AIM) theory (Bader 1994; Koch and Popelier 1995; Popelier 1998). According to this theory, the existence and the type of chemical interactions between two atoms can be determined by the electron density (ρ) and the Laplacian of the electron density ($\nabla^2\rho$). Corrections to the interaction energies to account for basis set superposition error (BSSE) were also calculated.

Results and discussion

Modification of ZnO NPs

ZnO NPs were synthesized and in situ modified by THMA, TOPO, HDA, and DDT from $Zn(Ac)_2$ solution. Compared with bare ZnO, ligand-modified ZnO NPs exhibited markedly different particle growth rates. This is reflected in the rate of change of the ZnO absorption band-edge present in the ZnO colloid solution UV–Vis absorption spectra given in Fig. 2.

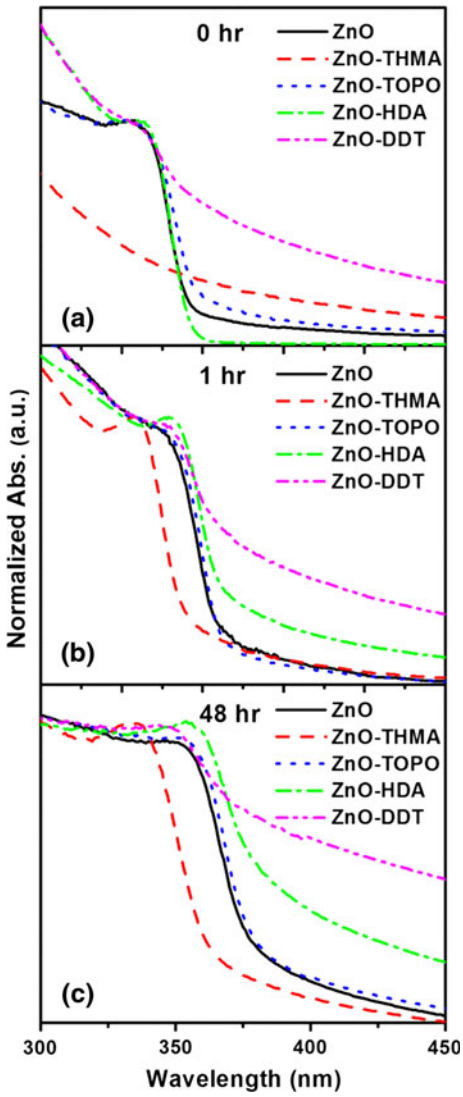

Fig. 2 Absorption spectra of ZnO colloids after annealing in ethanol for **a** 0 h, **b** 1 h, and **c** 48 h in the presence of different organic ligands

When HDA and DDT were used as capping ligands, the ZnO particles obviously grow faster than bare particles. In the case of TOPO, no significant difference was found when compared to synthesis without the capping ligand. However, the growth was significantly inhibited in the case of THMA.

Figure 2 shows the UV–Vis absorption spectra of as prepared ZnO colloids at different stages of the particle growth and capping by organic molecules on ZnO surfaces (Cozzoli et al. 2003; Kahn et al. 2005; Luo et al. 2009). Therefore, we propose THMA also interacts with the active sites on growth with each capping ligand. Well-defined absorption peaks were observed immediately upon injection of NaOH solution into the zinc precursor, except in the case of THMA. Then, the reaction solution was annealed in ethanol at 80 °C to investigate the ligand effects on particle growth. The absorption onset was red-shifted with increasing time, consistent with particle growth of these quantum-confined nanocrystals. By comparison, the absorbance peak of ZnO–THMA was actually observed to be blue-shifted, indicating smaller particle size. This could be attributed to the multifunctional groups ($-NH_2$ and –OH) present in THMA molecule. It was reported that amino and hydroxyl groups were often involved in the adsorption ZnO surfaces to decrease the surface energy and inhibit growth of the ZnO particles. This assumption will be discussed further in the computational section of this study.

In contrast to THMA, it was found that HDA and DDT modified ZnO NPs were larger than bare ZnO particles. These modified nanoparticles also showed a strong tendency to aggregate. The particle aggregation effect was particularly noticeable in these spectra as a long "tail" of high absorbance in the spectra at wavelengths longer than 350 nm. We suggest there are three types of interactions in the ZnO–ligand system: the interaction between ZnO crystal nuclei; the interactions between ZnO crystal nuclei and capping ligands and the interactions between capping ligands themselves. Without capping ligands, ZnO nuclei will grow to a certain size until the surface energy is stabilized or balanced with environment, consistent with coarsening models of growth where larger particles grow at the expense of smaller particles models (Wong et al. 2001). In the presence of capping ligands, such as THMA, the surface of ZnO crystallites will be stabilized by strong ligand bonds. In the case of HDA and DDT, stabilization will also occur, however one difference with these two species is that the effective diameter for a particular crystal nuclei will be far larger than THMA-capped ZnO nanoparticles. This is represented schematically in Fig. 3, where it is assumed that Van der Waals forces between the ligand straight alkyl-chains can result in a large percentage of all-trans configurations of the bound ligands for HDA and DDT in particular. Accordingly, aggregation is more likely to occur with HDA and DDT-capped ZnO nanoparticles due to interpenetration of the linear alkythiol and alkylamine ligand

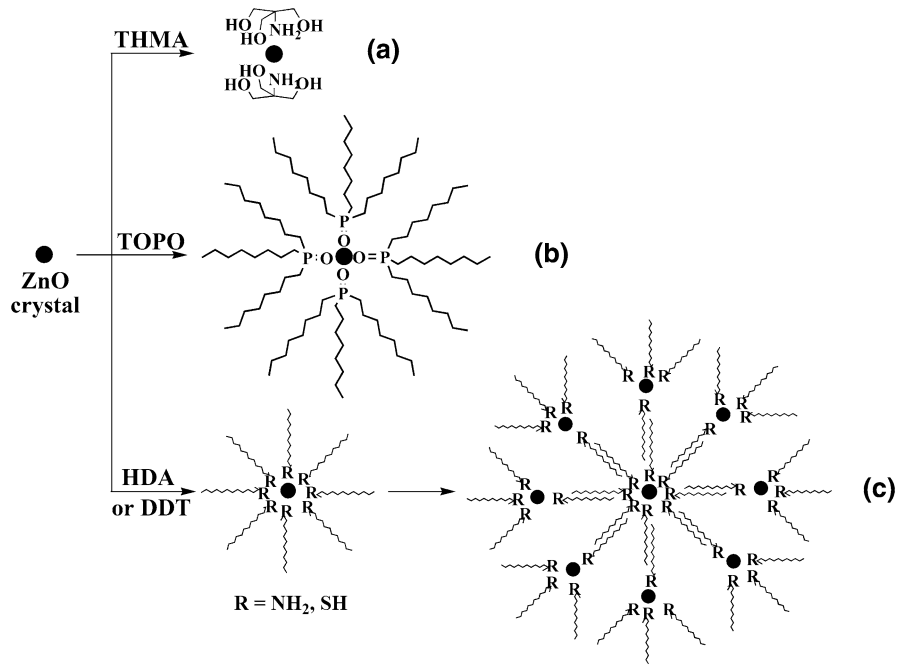

Fig. 3 Schematic diagram of the capping effect of different organic ligands on ZnO nanocrystal surface. *a* THMA, *b* TOPO, *c* HDA or DDT

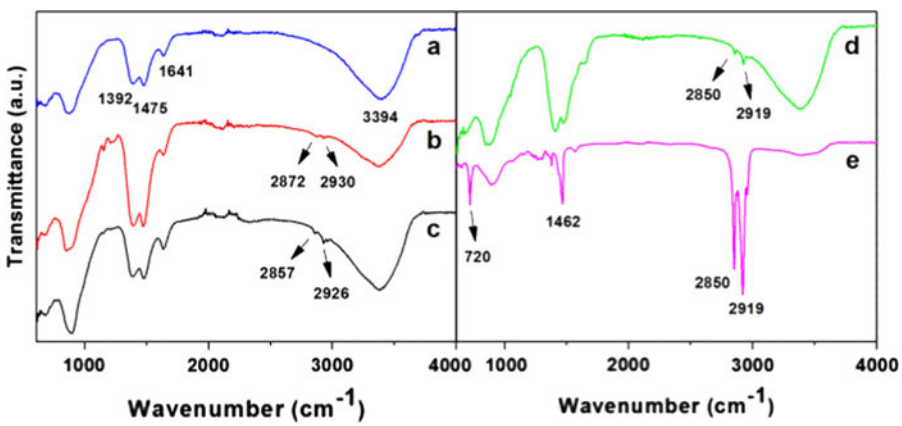

Fig. 4 The IR spectra of ZnO NPs with various capping ligands *a* bare ZnO, *b* ZnO–THMA, *c* ZnO–TOPO, *d* ZnO–HDA, and *e* ZnO–DDT

shells between adjacent particles (Heath et al. 1997). This interpenetration is likely to maximize dispersion attractions between ligand shells. Aggregation was clearly present in the UV–Vis of the linear alkythiol and alkylamine ligands in Fig. 2 and has been observed previously in the case of DDT-coated ZnO NPs where in fact linear chain aggregates were observed under similar synthetic conditions (Shortell et al. 2010). Decreased aggregation of particles was evident in the UV–Vis spectra of TOPO capped ZnO NPs. The structure of TOPO differs significantly from the linear chain HDA and DDT ligands, it has a tetrahedral structure with three long carbon chains. It is reasonable to assume that the major chemical binding interaction of TOPO with the ZnO surface is through the oxygen. The large space occupied by the hydrocarbon chains of each TOPO unit causes them to have a large molecular footprint at the ZnO surface. The density of TOPO molecules at ZnO surfaces is therefore likely to be lower than HDA or DDT which can close pack (Sadik et al. 2007). Decreased intermolecular interaction and the particle growth of TOPO functionalised ZnO NPs is therefore likely as well.

Structural and morphological characterization

The presence of capping ligands and the formation of ZnO NPs were supported by the FT-IR spectra as

shown in Fig. 4. The broad absorption bands near 3400 cm^{-1} represented O–H stretching vibration of absorbed water on the ZnO surface. The C=O stretching and C–O stretching vibration of acetate groups on ZnO surfaces have been reported to be around 1,585 and 1,444 cm^{-1}, respectively (Sakohara et al. 1992). It was also suggested these characteristic peaks varied slightly due to different bonding types of acetate and metal (Sakohara et al. 1998). It is notable that these observations were obtained using LiOH as base source while NaOH was used in our case. As shown in Fig. 4, three characteristic peaks (except Fig. 4e) around 1,400–1,640 cm^{-1} were observed and corresponded to acetate groups. This was supported by the results of a previous study which prepared ZnO samples from zinc acetate and NaOH as well (Wahab et al. 2007).

Compared with bare ZnO NPs, ZnO–THMA powder exhibited a weak C–H stretching vibration at about 2,872 and 2,930 cm^{-1} (Fig. 4b). The N–H stretching vibration of THMA and HDA ligands were overlapped by the O–H stretching vibration of hydroxyl groups on the ZnO surface (Fig. 4b, d). The bands around 2,857 and 2,926 cm^{-1} in Fig. 4c were attributed to the C–H stretching vibration of ZnO–TOPO. Figure 4d, e exhibited clear C–H stretching vibration peaks assigned to HDA and DDT at around 2850 cm^{-1} and 2,919 cm^{-1}. The strong C–H stretching vibration peak in ZnO–DDT indicates that DDT was heavily absorbed on ZnO surfaces with respect to other ligands. The C–H bending and CH_2 rocking vibrations of DDT were identified at around 1,462 and 720 cm^{-1}, respectively. The C=O and C–O stretching vibrations of acetate group were overlapped by the C–H bending band of DDT in Fig. 4e. In addition, all of the capping ligands (except DDT) could be removed by rinsing ZnO powder with ethanol and deionized water repeatedly. This is critical for those applications where organic ligands might interfere with and weaken ZnO's useful properties, optical properties in particular (Wang et al. 2009).

Figure 5 shows the XRD patterns of ZnO NPs which were annealed in ethanol for 72 h at around 80 °C. By comparing the diffraction peak positions with those reported in the International Crystallographic data table (ICDD), all samples were assigned to be hexagonal wurtzite crystal structures. It is observed that the XRD peak full width at maximum (FWHM) was widened by THMA while sharpened by DDT.

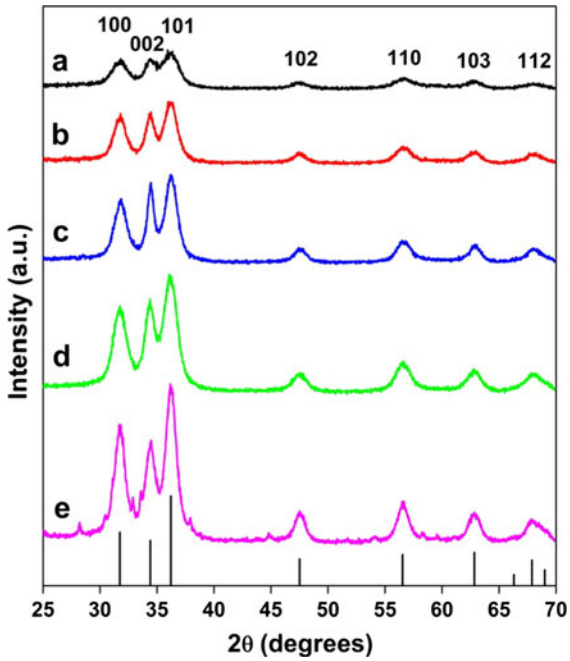

Fig. 5 XRD patterns of ZnO NPs along with the wurtzite ZnO diffraction lines *a* ZnO–THMA, *b* bare ZnO, *c* ZnO–TOPO, *d* ZnO–HDA, and *e* ZnO–DDT

Table 1 Values of the average particle size (*d*) calculated by Scherrer's Formula for the (101) and (102) XRD peaks of ZnO powders

Samples	$d_{(101)}$ (nm)	$d_{(102)}$ (nm)
Bare ZnO	6.8	6.3
ZnO–THMA	5.3	3.6
ZnO–HDA	6.9	6.9
ZnO–TOPO	7.3	7.6
ZnO–DDT	8.9	8.7

The average particle size, *d*, was estimated by using the Scherrer formula. Table 1 shows the primary crystallite size calculated from the full width at half-maximum of the (101) and (102) diffraction peaks. It is shown that apart from ZnO–THMA, other ZnO nanoparticle sizes along the (101) planes are similar with that of the (102) planes, indicating almost spherical particles. The particle size of ZnO–THMA was smaller than bare ZnO powder while other ZnO NPs were slightly larger. This trend in ZnO particle sizes was consistent with trends observed in the measurement of UV–Vis absorption spectra. We are careful to note that although we have called the

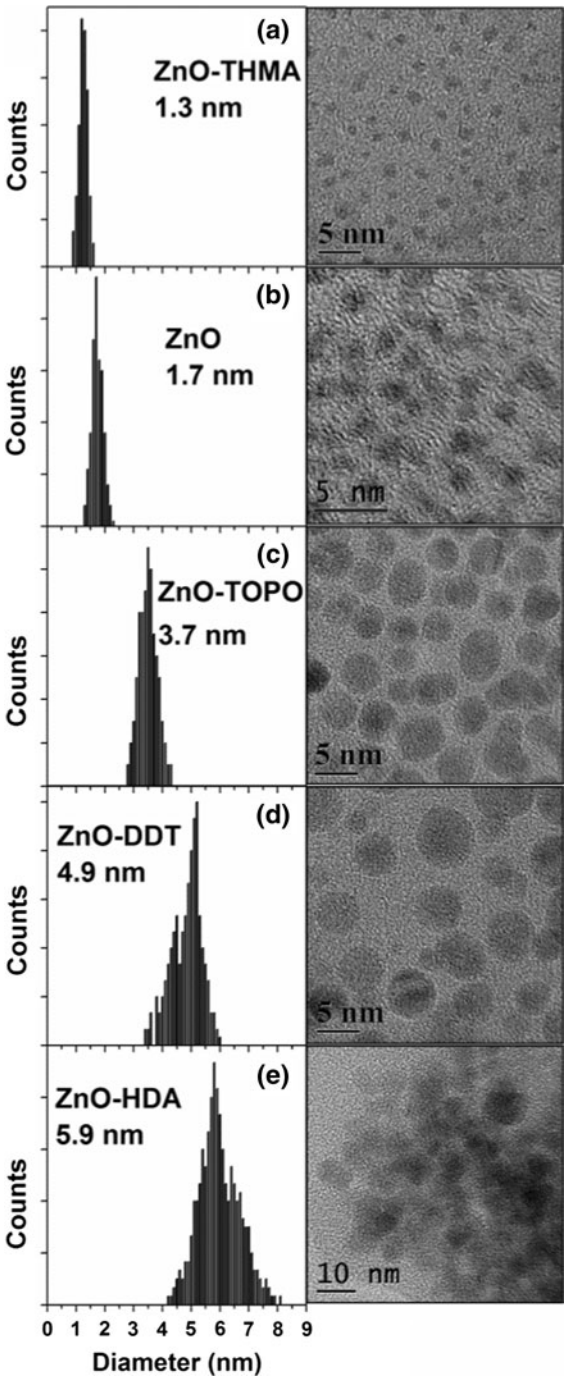

Fig. 6 TEM images and size distribution analyses of ZnO nanocrystals after refluxing in ethanol for 30 min **a** ZnO–THMA, **b** bare ZnO, **c** ZnO–TOPO, **d** ZnO–DDT, and **e** ZnO–HDA

unmodified sample "Bare ZnO", acetate ligands from the hydrolysed precursor readily bind to ZnO surfaces and are in fact essential to keep the colloid size small

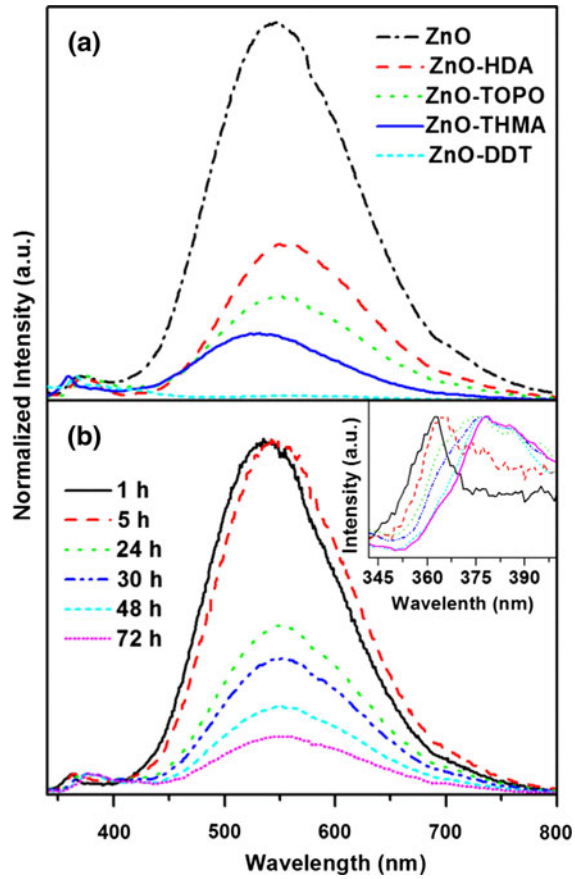

Fig. 7 Normalized PL emission spectra of as prepared ZnO colloid annealed at 80 °C **a** modified with different capping ligands (THMA, TOPO, HDA, and DDT) and annealed for 48 h, **b** ZnO–TOPO colloid annealed for various time from 1 h to 72 h and the enlarged region of 342–400 nm (*inset*)

and size distribution narrow. Strong evidence of acetate playing a major role in colloid stabilization and growth can be found in earlier study focused on developing the acetate hydrolysis method. See for example, study by Spanhel (2006), Meulenkamp (1998) and Anderson and coauthors (1998, 1992).

The morphology of the particles was confirmed by TEM measurement after annealing for 30 min in ethanol (Fig. 6). Particle size distributions were also calculated by measuring the particle diameters in the TEM images from >100 particles for each sample. In the absence of capping ligands, ZnO crystals appeared indistinct and non-spherical, with a mean size of around 1.7 nm (Fig. 6b). In Fig. 6a, nanoparticles appeared rather well separated on the grid and without tendency of aggregation because of the THMA capping. The average particle size of ZnO–THMA

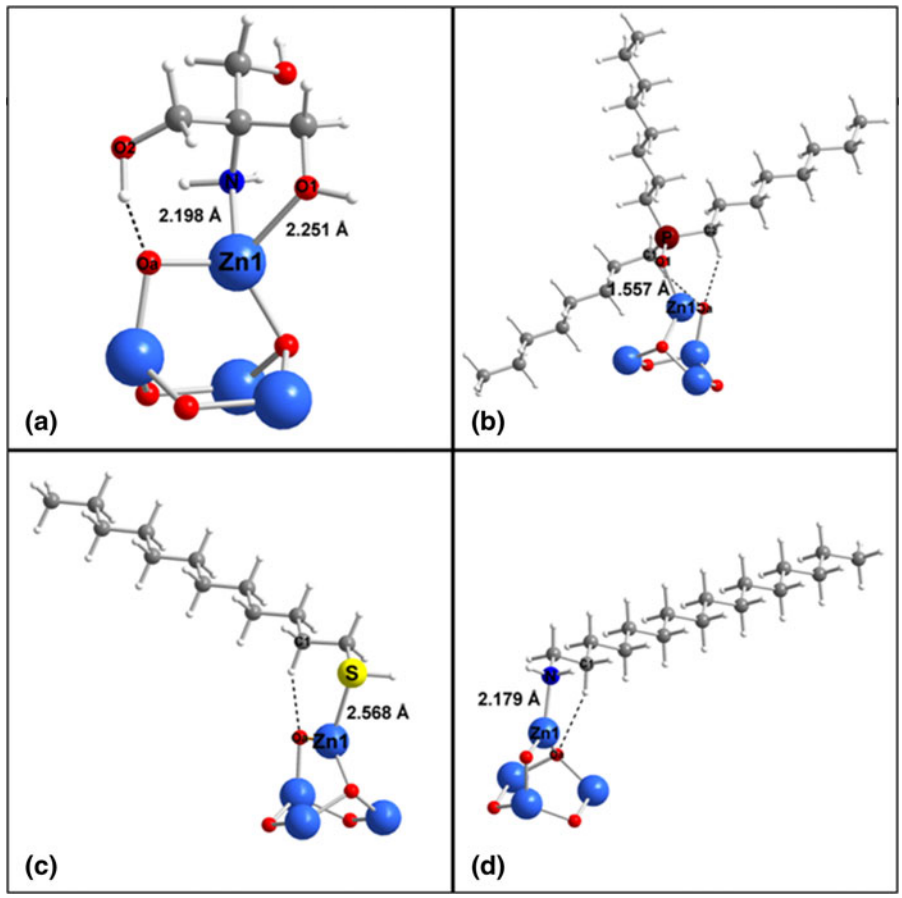

Fig. 8 Optimized geometries of capping ligands adsorbed on the Zn_4O_4 surface obtained at the B3LYP/LanL2DZ level of theory. **a** Z–TH system, **b** Z–TO system, **c** Z–DT system, and **d** Z–HD system

was reduced to around 1.3 nm. In contrast to these small particle size distributions, nanoparticles modified by TOPO, DDT and HDA all exhibited bigger sizes and broader size distributions. In addition, the TEM image of ZnO–HDA (Fig. 6e) shows obvious signs of significant particle aggregation, in agreement with the results of the adsorption spectra and the XRD data fitting.

Photoluminescence

In Fig. 7, the PL spectra of ZnO colloid modified with different ligands (THMA, TOPO, HDA, and DDT) and the spectra of ZnO–TOPO colloid at different annealed time are reported. As shown in Fig. 7a, typical PL spectra of ZnO colloid consisted of a broad green emission attributed to surface defect states and a relatively narrow UV emission ascribed to band-edge recombination (Kroger and Vink 1954; Anpo and Kubokawa 1984; Sakohara et al. 1992). These spectra were measured for the as prepared ZnO colloid after annealing in ethanol at 80 °C for 48 h. By comparison, both UV and green emissions of ZnO–THMA colloid were blue-shifted with respect to other samples, indicating smaller particle size in the quantum confinement regime (van Dijken et al. 2001). Compared with bare ZnO colloid, the intensity of green emission was decreased for ligand-capped ZnO NPs. Particularly, the green emission of ZnO–DDT was almost entirely quenched, in agreement with the intensive characteristic peaks of DDT in FT-IR spectra. This decrease of green emission intensity implied reduction of surface defects. We suggest that the oxygen vacancies at the ZnO surface were passivated by ligands, consistent with similar PL studies of dodecylamine (DDA) (Norberg and Gamelin 2005) or TOPO (Shim and Guyot Sionnest 2001) capped ZnO nanocrystals.

Figure 7b presents the normalized PL emission spectra of ZnO–TOPO colloid in ethanol after

Table 2 Electron density (ρ), Laplacian of the electron density ($\nabla^2\rho$), H···Y and X···Y distances (Å), and ∠X–H–Y bond angles of the formed bonds for the Zn_4O_4–ligand and $Zn_{18}O_{18}$–ligand systems calculated at the B3LYP/LanL2DZ level of theory

Bonds	Z–TH			Z–TH–L		
	$\rho(\nabla^2\rho)$	∠X–H–Y	H···Y(X···Y)	$\rho(\nabla^2\rho)$	∠X–H–Y	H···Y(X···Y)
N···Zn1	0.051195 (0.177667)		(2.198)	0.049483 (0.160077)		(2.216)
O1···Zn1	0.028728 (0.153888)		(2.251)			
O1···Zn2				0.026122 (0.090443)		(2.393)
O2–H···Oa	0.044548 (0.368253)	162.2	1.511	0.059425 (0.173788)	164.7	1.596
O1–H···Ob				0.049174 (0.154834)	138.2	1.705
	Z–TO			Z–TO–L		
	$\rho(\nabla^2\rho)$	∠X–H–Y	H···Y(X···Y)	$\rho(\nabla^2\rho)$	∠X–H–Y	H···Y(X···Y)
O1···Zn1	0.059788 (0.304820)		(2.038)	0.050490 (0.210971)		(2.117)
C1–H···Oa	0.015587 (0.057457)	140.9	2.254	0.017728 (0.052152)	152.9	2.232
C2–H···Oa	0.014114 (0.051235)	140.9	2.293			
C3–H···Zn2				0.009435 (0.035839)	105.6	2.587
	Z–DT			Z–DT–L		
	$\rho(\nabla^2\rho)$	∠X–H–Y	H···Y (X···Y)	$\rho(\nabla^2\rho)$	∠X–H–Y	H···Y (X···Y)
S···Zn1	0.039453 (0.075146)		(2.568)	0.033690 (0.070484)		(2.627)
C1–H···Oa	0.016439 (0.051004)	153.1	2.241	0.023805 (0.090594)	145.4	2.074
C2–H···Ob				0.014177 (0.062915)	160.8	2.325
	Z–HD			Z–HD–L		
	$\rho(\nabla^2\rho)$	∠X–H–Y	H···Y(X···Y)	$\rho(\nabla^2\rho)$	∠X–H–Y	H···Y(X···Y)
N···Zn1	0.054199 (0.182129)		(2.179)	0.049074 (0.160313)		(2.213)
C1–H···Oa	0.008414 (0.027419)	149.0	2.630			
N–H···Oa				0.020226 (0.076019)	120.4	2.124

annealing at 80 °C for certain times. It was observed that the green emission intensity gradually reduced with the annealing time, consistent with the particle growth process in previous studies (Wood et al. 2003; van Dijken et al. 2001; Norberg and Gamelin 2005). In addition, as increasing the annealing time, the UV emission red-shifted slightly (inset figure), in agreement with the red-shift of absorption peaks. This red-shift caused by annealing of the ZnO material can be attributed to particle coarsening (growth) during the anneal step (Spanhel and Anderson 1991; Sakohara et al. 1992; Morfa et al. 2010).

Simulation of ligands adsorbed on ZnO

The optimized structures of capping ligands adsorbed on the Zn_4O_4 fragment are illustrated in Fig. 8. The main purpose for the calculation of this model was to investigate interactions between capping ligands and the low-coordination number, active sites of ZnO crystal nuclei, and in the case of corner sites (which can be considered as sites present on the (0001) surfaces), to compare ligand-binding effects. The calculated interaction distances (r) (between ligands and ZnO fragment) with the corresponding electron density ($\rho(r)$) and Laplacian of the electron density ($\nabla^2\rho(r)$) values are shown in Table 2. In the Z–TH system, chemical bonds are formed between N, O atoms of THMA, and the Zn atom of the Zn_4O_4 fragment. The Zn···N and Zn···O distances are 2.20 and 2.25 Å, respectively, and these bonds are created with a two-coordinated Zn^{2+} site. The Z–TH system is further stabilized by the formation of an O–H···O type hydrogen bond, possessing 1.51 Å H···O distance. The values of the electron density for Zn···N, Zn···O, and H···O are 0.051, 0.029 and 0.045 e/au^3, respectively. Therefore, the strongest and weakest interactions in Z–TH system come from Zn···N and H···O bonds, while the Zn···O appears to give only a moderate contribution to stabilization of the system. Compared with Z–TH system, in each of other systems, there is only one chemical bond created with each Zn^{2+} site,

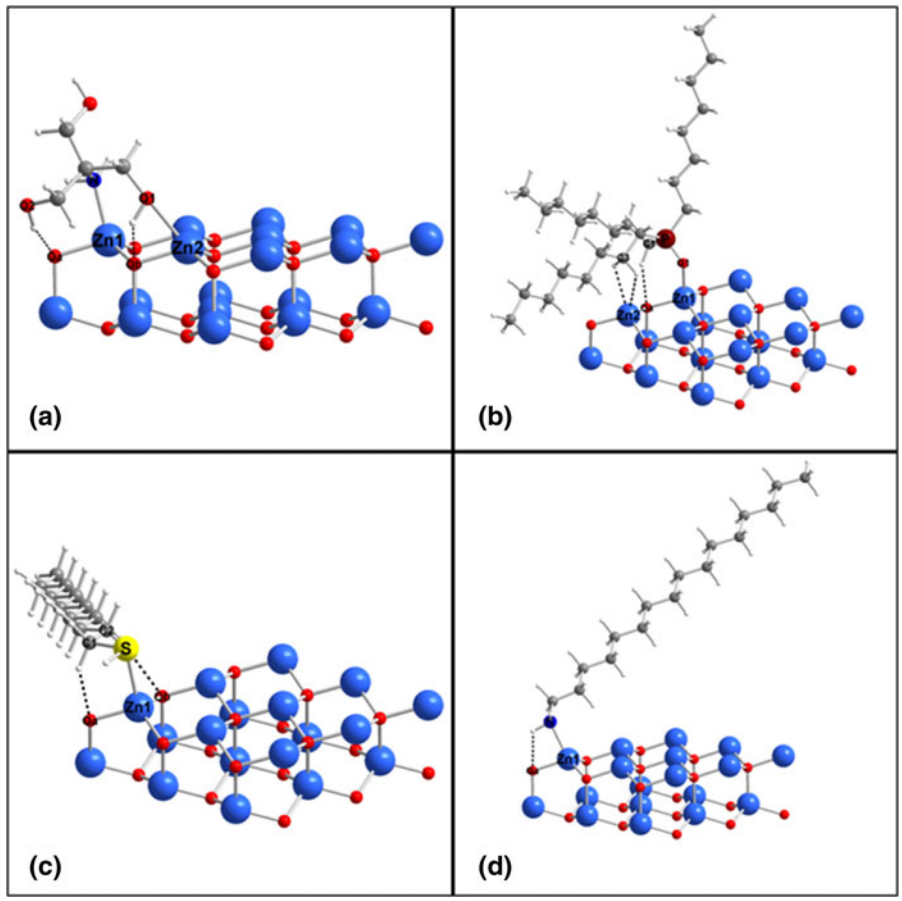

Fig. 9 Optimized geometries of capping ligands adsorbed on the $Zn_{18}O_{18}$ surface (0001) obtained at the B3LYP/LanL2DZ level of theory. **a** Z–TH–L system, **b** Z–TO–L system, **c** Z–DT–L system, and **d** Z–HD–L system

accompanied by hydrogen bonds of varying strength, depending on adsorbed species. For Z–TO, one chemical bond between O of TOPO and the Zn^{2+} site and two C–H···O hydrogen bonds are created. The Zn_4O_4 cluster was mainly stabilized by the formation of the Zn···O bond, as indicated by the electron density value of Zn···O bond (0.060 e/au^3) which is almost four times larger than that of hydrogen-bond interactions (0.016 and 0.014 e/au^3). With Z–DT, the significant interaction with the Zn_4O_4 fragment was the chemical bond between the S atom of DDT and the Zn^{2+} site of the ZnO cluster. Values of the electron density of the Zn···S bond and the C–H···O hydrogen bond were 0.040 e/au^3 and 0.016 e/au^3, respectively. In the case of Z–HD system, a N···Zn chemical bond and C–H···O hydrogen bond formed between HDA and the Zn_4O_4 model, where the N···Zn bond clearly provides the main contribution toward the intermolecular interaction with the ZnO model surface. By comparing the electron density values of the formed bonds in these systems, it was obvious the interaction was highest for the Z–TH system while the interaction was lowest for the Z–HD system.

Figure 9 exhibits the optimized structures of capping ligands adsorbed on the Zn-terminated $Zn_{18}O_{18}$ cluster (0001 surface). It was shown THMA interacted with two top Zn atoms and two O atoms at the boundary of the second layer. The main interaction comes from the formation of hydrogen bonds involving the second layer O atoms. This stabilized role of these O atoms was also confirmed for the adsorption of methanol on (0001) ZnO surface (Vohs and Barteau 1986, 1989). It was notable the Zn1···N and Zn1···O1 bonds in Z–TH system were slightly stronger than that in Z–TH–L system (the differences in ρ are 0.002 and 0.003 e/au^3, respectively). This is because N and O1 atoms were bonded with the same Zn atom in Z–TH system, forming a stable five-membered ring. In Z–TH–L system, N atom was bonded with Zn1 while O1 atom is bonded with adjacent Zn2 atom, forming a less

stable seven-membered ring. For Z–TO–L system, the main interaction is contributed by the formation of Zn1···O1 bond in which the P=O group of TOPO is involved. The P=O group has been recently reported to react with ZnO clusters with different sizes (Paukku et al. 2009). The difference between Z–TO and Z–TO–L systems is that C3–H···Zn2 bonds were formed in latter system, although they were very weak and negligible. Compared with Z–DT system, one more hydrogen bond (C2–H···Ob) was formed in Z–DT–L system. However, the Zn1···S chemical bond was relative weaker in the Z–DT–L system (the difference in ρ is $\sim$0.006 e/au^3, and the difference in $\nabla^2\rho$ is $\sim$0.005 e/au^5). For Z–HD–L system, the Zn1···N bond was weaker than that in the Z–HD system, while N–H···O a hydrogen bond was formed.

Interaction energies

Interaction energies (E_I) were calculated by taking the difference between the energy of the interacting system

(E_{ZnO-L}) and the sum of the energies of ZnO cluster (E_{ZnO}) and isolated capping ligand (E_L) with Eq. (1):

$$E_I = E_{ZnO-L} - E_{ZnO} - E_L \quad (1)$$

In addition, the basis set superposition error (BSSE) was also calculated, using the Boys–Bernardi counterpoise method (Boys and Bernardi 1970). The corrected interaction energies (E_{I+BSSE}) were therefore calculated with Eq. (2):

$$E_{I+BSSE} = E_I + E_{BSSE} \quad (2)$$

Table 3 presents the corrected interaction energies and the basis set superposition error for all the interacting systems. For both Zn_4O_4–ligand and $Zn_{18}O_{18}$–ligand systems, the interaction energies decreased in the order of: THMA > TOPO > HDA > DDT. The interaction energy of Z–TH was determined to be −152 kJ/mol, which was much higher than Z–DT system (−43.5 kJ/mol). It was also shown that for the systems with same ligands, the interaction energies decreased as the extension of ZnO cluster. For $Zn_{18}O_{18}$–ligand systems, the highest and lowest interaction energies were −85.2 kJ/mol (Z–TH–L) and −37.4 kJ/mol (Z–DT–L), respectively. Similar results were found in the simulation of HCOOH adsorbed on ZnO surfaces, which has shown that heats of dissociative adsorption of HCOOH decreased as the Zn_nO_n ($n = 4, 9, 16, 25, 36, 49$) cluster extended (Zhanpeisov et al. 1997). These findings were consistent with our experimental results, which show that THMA significantly inhibited the growth of ZnO particles. We suggested this is due to the strong adsorption of THMA on ZnO crystal nucleus, therefore stabilize the crystal facets and prevent the particle growth.

Table 3 Interaction energy values (kJ/mol) of the Zn_4O_4–ligand and $Zn_{18}O_{18}$–ligand systems obtained at the B3LYP/LanL2DZ level of theory

	Z–TH	Z–TO	Z–HD	Z–DT
E_{I+BSSE}	−152	−101	−72.5	−43.5
E_{BSSE}	26.0	19.3	13.4	9.70
	Z–TH–L	Z–TO–L	Z–HD–L	Z–DT–L
E_{I+BSSE}	−85.2	−78.9	−54.5	−37.4
E_{BSSE}	45.0	28.2	14.8	11.8

Conclusions

In conclusion, the effect of ligand structures on the growth of ZnO nanoparticles has been investigated experimentally and theoretically. Ab initio DFT calculations indicated that small molecules with multi-functional groups (THMA) adsorb to the ZnO surface with stronger bonds and higher interaction energy. Interactions between ZnO clusters and long carbon-chain ligands (such as DDT and HDA) were relatively weak in comparison. This explained our experimental observations that THMA significantly inhibited the growth of ZnO nanoparticles. It is reasonable to assume that THMA interacted with ZnO crystal nuclei to stabilize the crystal facets and prevented the particle growth. The observation of significant ZnO nanoparticle aggregation effects occurring in the case of ZnO–DDT and ZnO–HDA particles, suggests Van der Waals forces between the DDT or HDA linear hydrocarbon chains weight the particle-stabilization effects of these ligands. This is likely since the strength of the Van der Waals force scales with the length of carbon chains in organic compounds. This scenario was also supported by investigating the TOPO-capped ZnO, which showed only a slight ligand-effect on the particle growth because of weakened Van der Waals interactions arising from the steric effect of adjacent TOPO

molecules. This study provides a simple and efficient way to control the size of ZnO nanoparticles, but also explains the effects of ligand structures on ZnO nanoparticles which could be employed toward the morphology control of metal oxide nanoparticles. It also gives insight into the correlation between the nature of binding of the ligands and ZnO nanoparticles which could be used to guide the synthesis of similar metal oxide nanomaterials systems.

Acknowledgments This study has been supported by the Queensland Government through the NIRAP project "Solar Powered Nanosensors". We thank High Performance Computing and Research Support (HPC) team, Queensland University of Technology for the support on the calculation work. We also thank Mr. Xiaoyue Liu, Southwest University, China, for his help with AIM analysis. Jin thanks the China Scholarship Council (CSC) for providing a scholarship for PhD research.

References

Anpo M, Kubokawa Y (1984) Photoluminescence of zinc oxide powder as a probe of electron–hole surface processes. J Phys Chem 88(23):5556–5560

Bader R (1994) Atoms in molecules: a quantum theory. Oxford University Press, New York

Bahnemann DW, Kormann C, Hoffmann MR (1987) Preparation and characterization of quantum size zinc oxide: a detailed spectroscopic study. J Phys Chem 91(14): 3789–3798

Ballerini G, Ogle K, Barthés-Labrousse MG (2007) The acid–base properties of the surface of native zinc oxide layers: an XPS study of adsorption of 1,2-diaminoethane. Appl Surf Sci 253(16):6860–6867

Becke AD (1993) Density-functional thermochemistry. III. The role of exact exchange. J Chem Phys 98(7):5648–5652

Boys SF, Bernardi F (1970) The calculation of small molecular interactions by the differences of separate total energies. Some procedures with reduced errors. Mol Phys 19(4):553–566

Choi KJ, Jang HW (2010) One-dimensional oxide nanostructures as gas-sensing materials: review and issues. Sensors 10(4):4083–4099

Cozzoli PD, Curri ML, Agostiano A, Leo G, Lomascolo M (2003) ZnO nanocrystals by a non-hydrolytic route: synthesis and characterization. J Phys Chem B 107(20): 4756–4762

Deng C, Hu H, Shao G, Han C (2010) Facile template-free sonochemical fabrication of hollow ZnO spherical structures. Mater Lett 64(7):852–855

Dev A, Panda SK, Kar S, Chakrabarti S, Chaudhuri S (2006) Surfactant-assisted route to synthesize well-aligned ZnO nanorod arrays on sol–gel-derived ZnO thin films. J Phys Chem B 110(29):14266–14272

Dvorak J, Jirsak T, Rodriguez JA (2001) Fundamental studies of desulfurization processes: reaction of methanethiol on ZnO and Cs/ZnO. Surf Sci 479(1–3):155–168

Forleo A, Francioso L, Capone S, Siciliano P, Lommens P, Hens Z (2010) Synthesis and gas sensing properties of ZnO quantum dots. Sens Actuators B 146(1):111–115

Frisch MJ, Trucks GW, Schlegel HB, Scuseria GE, Robb MA, Cheeseman JR, Scalmani G, Barone V, Mennucci B, Petersson GA, Nakatsuji H, Caricato M, Li X, Hratchian HP, Izmaylov AF, Bloino J, Zheng G, Sonnenberg JL, Hada M, Ehara M, Toyota K, Fukuda R, Hasegawa J, Ishida M, Nakajima T, Honda Y, Kitao O, Nakai H, Vreven T, Montgomery Jr JA, Peralta JE, Ogliaro F, Bearpark M, Heyd JJ, Brothers E, Kudin KN, Staroverov VN, Kobayashi R, Normand J, Raghavachari K, Rendell A, Burant JC, Iyengar SS, Tomasi J, Cossi M, Rega N, Millam NJ, Klene M, Knox JE, Cross JB, Bakken V, Adamo, C, Jaramillo J, Gomperts R, Stratmann RE, Yazyev O, Austin AJ, Cammi R, Pomelli C, Ochterski JW, Martin RL, Morokuma K, Zakrzewski VG, Voth GA, Salvador P, Dannenberg JJ, Dappric HS, Daniels AD, Farkas Ö, Foresman JB, Ortiz JV, Cioslowski J, Fox DJ (2009) Gaussian 09, revision A.1. Gaussian Inc., Wallingford

Hay PJ, Wadt WR (1985a) Ab initio effective core potentials for molecular calculations. Potentials for K to Au including the outermost core orbitals. J Chem Phys 82(1):299

Hay PJ, Wadt WR (1985b) Ab initio effective core potentials for molecular calculations. Potentials for the transition metal atoms Sc to Hg. J Chem Phys 82(1):270

Heath JR, Knobler CM, Leff DV (1997) Pressure/temperature phase diagrams and superlattices of organically functionalized metal nanocrystal monolayers: the influence of particle size, size distribution, and surface passivant. J Phys Chem B 101(2):189–197

Huynh WU, Dittmer JJ, Alivisatos AP (2002) Hybrid nanorod-polymer solar cells. Science 295(5564):2425–2427

Irrera S, Costa D, Marcus P (2009) DFT periodic study of adsorption of glycine on the (0001) surface of zinc terminated ZnO. J Mol Struct (Theochem) 903(1–3):49–58

Jian D, Gao PX, Cai W, Allimi BS, Pamir Alpay S, Ding Y, Wang ZL, Brooks C (2009) Synthesis, characterization, and photocatalytic properties of ZnO/(La, Sr)CoO3 composite nanorod arrays. J Mater Chem 19(7):970–975

Jouane Y, Colis S, Schmerber G, Kern P, Dinia A, Heiser T, Chapuis YA (2011) Room temperature ZnO growth by rf magnetron sputtering on top of photoactive P3HT: PCBM for organic solar cells. J Mater Chem 21(6):1953–1958

Kahn M, Monge M, Collière V, Senocq F, Maisonnat A, Chaudret B (2005) Size- and shape-control of crystalline zinc oxide nanoparticles: a new organometallic synthetic method. Adv Funct Mater 15(3):458–468

Klabunde KJ, Stark J, Koper O, Mohs C, Park DG, Decker S, Jiang Y, Lagadic I, Zhang D (1996) Nanocrystals as stoichiometric reagents with unique surface chemistry. J Phys Chem 100(30):12142–12153

Koch U, Popelier PLA (1995) Characterization of C–H–O hydrogen bonds on the basis of the charge density. J Phys Chem 99(24):9747–9754

Kroger FA, Vink HJ (1954) The origin of the fluorescence in self-activated ZnS, CdS, and ZnO. J Chem Phys 22(2):250–252

Li Y, Li X, Yang C, Li Y (2004) Ligand-controlling synthesis and ordered assembly of ZnS nanorods and nanodots. J Phys Chem B 108(41):16002–16011

Liao L, Lu HB, Li JC, He H, Wang DF, Fu DJ, Liu C, Zhang WF (2007) Size dependence of gas sensitivity of ZnO nanorods. J Phys Chem C 111(5):1900–1903

Liu XH, Zhang J, Wang LW, Yang TL, Guo XZ, Wu SH, Wang SR (2011) 3D hierarchically porous ZnO structures and their functionalization by Au nanoparticles for gas sensors. J Mater Chem 21(2):349–356

Lü X, Xu X, Wang N, Zhang Q, Ehara M, Nakatsuji H (1998) Cluster modeling of metal oxides: how to cut out a cluster? Chem Phys Lett 291(3–4):445–452

Luo B, Rossini JE, Gladfelter WL (2009) Zinc oxide nanocrystals stabilized by alkylammonium alkylcarbamates. Langmuir 25(22):13133–13141

Mao J, Li XL, Qin WJ, Niu KY, Yang J, Ling T, Du XW (2010) Control of the morphology and optical properties of ZnO nanostructures via hot mixing of reverse micelles. Langmuir 26(17):13755–13759

Martins JBL, Longo E, Salmon ODR, Espinoza VAA, Taft CA (2004) The interaction of H2, CO., CO2, H2O and NH3 on ZnO surfaces: an Oniom study. Chem Phys Lett 400(4–6): 481–486

Meulenkamp EA (1998) Synthesis and growth of ZnO nanoparticles. J Phys Chem B 102(29):5566–5572

Meyer B, Rabaa H, Marx D (2006) Water adsorption on ZnO(1010): from single molecules to partially dissociated monolayers. PCCP 8(13):1513–1520

Morfa AJ, Beane G, Mashford B, Singh B, Della Gaspera E, Martucci A, Mulvaney P (2010) Fabrication of ZnO thin films from nanocrystal inks. J Phys Chem C 114(46): 19815–19821

Neubauer A, Szarko JM, Bartelt AF, Eichberger R, Hannappel T (2011) Photophysical study of perylene/TiO2 and perylene/ZnO varying interfacial couplings and the chemical environment. J Phys Chem C 115(13): 5683–5691

Norberg NS, Gamelin DR (2005) Influence of surface modification on the luminescence of colloidal ZnO nanocrystals. J Phys Chem B 109(44):20810–20816

Norris BJ et al (2003) Spin-coated zinc oxide transparent transistors. J Phys D Appl Phys 36(20):L105

Pacholski C, Kornowski A, Weller H (2002) Angew Chem Int Ed 41(7):1188–1191

Park K, Zhang Q, Garcia BB, Cao G (2011) Effect of annealing temperature on TiO2–ZnO core–shell aggregate photoelectrodes of dye-sensitized solar cells. J Phys Chem C 115(11):4927–4934

Parr RG, Yang W (1994) Density-functional theory of atoms and molecules. Oxford University Press, New York

Paukku Y, Michalkova A, Leszczynski J (2009) Quantum-chemical comprehensive study of the organophosphorus compounds adsorption on zinc oxide surfaces. J Phys Chem C 113(4):1474–1485

Pesika NS, Hu Z, Stebe KJ, Searson PC (2002) Quenching of growth of ZnO nanoparticles by adsorption of octanethiol. J Phys Chem B 106(28):6985–6990

Popelier PLA (1998) Characterization of a dihydrogen bond on the basis of the electron density. J Phys Chem A 102(10):1873–1878

Qian L, Zheng Y, Xue J, Holloway PH (2011) Stable and efficient quantum-dot light-emitting diodes based on solution-processed multilayer structures. Nat Photonics 5(9): 543–548

Sadik PW, Pearton SJ, Norton DP, Lambers E, Ren F (2007) Functionalizing Zn- and O-terminated ZnO with thiols. J Appl Phys 101(10):104514

Sakohara S, Tickanen LD, Anderson MA (1992) Luminescence properties of thin zinc oxide membranes prepared by the sol-gel technique: change in visible luminescence during firing. J Phys Chem 96(26):11086–11091

Sakohara S, Ishida M, Anderson MA (1998) Visible luminescence and surface properties of nanosized ZnO colloids prepared by hydrolyzing zinc acetate. J Phys Chem B 102(50):10169–10175

Shim M, Guyot Sionnest P (2001) Organic-capped ZnO nanocrystals: synthesis and n-type character. JACS 123(47): 11651–11654

Shortell MP, Liu HW, Zhu H, Jaatinen EA, Waclawik ER (2010) Formation of one-dimensional capped ZnO nanoparticle assemblies at the air/water interface. Langmuir 26(18):14472–14478

Spanhel L (2006) Colloidal ZnO nanostructures and functional coatings: a survey. J Sol Gel Sci Technol 39(1):7–24

Spanhel L, Anderson MA (1991) Semiconductor clusters in the sol-gel process: quantized aggregation, gelation, and crystal growth in concentrated zinc oxide colloids. JACS 113(8):2826–2833

Usui H, Shimizu Y, Sasaki T, Koshizaki N (2004) Photoluminescence of ZnO nanoparticles prepared by laser ablation in different surfactant solutions. J Phys Chem B 109(1):120–124

van Dijken A, Makkinje J, Meijerink A (2001) The influence of particle size on the luminescence quantum efficiency of nanocrystalline ZnO particles. J Lumin 92(4):323–328

Vohs JM, Barteau MA (1986) Conversion of methanol, formaldehyde and formic acid on the polar faces of zinc oxide. Surf Sci 176(1–2):91–114

Vohs JM, Barteau MA (1989) Dehydration and dehydrogenation of ethanol and 1-propanol on the polar surfaces of zinc oxide. Surf Sci 221(3):590–608

Wadt WR, Hay PJ (1985) Ab initio effective core potentials for molecular calculations. Potentials for main group elements Na to Bi. J Chem Phys 82(1):284

Wahab R, Ansari SG, Kim YS, Seo HK, Kim GS, Khang G, Shin HS (2007) Low temperature solution synthesis and characterization of ZnO nano-flowers. Mater Res Bull 42(9):1640–1648

Wahlström E, Vestergaard EK, Schaub R, Rønnau A, Vestergaard M, Lægsgaard E, Stensgaard I, Besenbacher F (2004) Electron transfer-induced dynamics of oxygen molecules on the TiO2(110) surface. Science 303(5657):511–513

Wang J, Tsuzuki T, Sun L, Wang X (2009) Reducing the photocatalytic activity of zinc oxide quantum dots by surface modification. J Am Ceram Soc 92(9):2083–2088

Westermark K, Rensmo H, Lees AC, Vos JG, Siegbahn H (2002) Electron spectroscopic studies of bis-(2,2′-bipyridine)-(4,4′-dicarboxy-2,2′-bipyridine)-ruthenium(II) and bis-(2,2′-bipyridine)-(4,4′-dicarboxy-2,2′-bipyridine)-osmium(II) adsorbed on nanostructured TiO_2 and ZnO surfaces. J Phys Chem B 106(39):10108–10113

Wong EM, Hoertz PG, Liang CJ, Shi BM, Meyer GJ, Searson PC (2001) Influence of organic capping ligands on the growth kinetics of ZnO nanoparticles. Langmuir 17(26): 8362–8367

Wood A, Giersig M, Hilgendorff M, Vilas-Campos A, Liz-Marzan LM, Mulvaney P (2003) Size effects in ZnO: the cluster to quantum dot transition. Aust J Chem 56(10): 1051–1057

Wu JJ, Liu SC (2002) Low-temperature growth of well-aligned ZnO nanorods by chemical vapor deposition. Adv Mater 14(3):215–218

Xing X, Zheng K, Xu H, Fang F, Shen H, Zhang J, Zhu J, Ye C, Cao G, Sun D, Chen G (2006) Synthesis and electrical properties of ZnO nanowires. Micron 37(4):370–373

Xu H, Zhang RQ, Tong SY (2010a) Interaction of O_2, H_2O, N_2, and O_3 with stoichiometric and reduced ZnO(1010) surface. Phys Rev B 82(15):155326

Xu LL, Li ZM, Cai QH, Wang HX, Gao H, Lv W, Liu J (2010b) Precursor template synthesis of three-dimensional mesoporous ZnO hierarchical structures and their photocatalytic properties. CrystEngComm 12(7):2166–2172

Yin M, Gu Y, Kuskovsky IL, Andelman T, Zhu Y, Neumark GF, O'Brien S (2004) Zinc oxide quantum rods. JACS 126(20):6206–6207

Zhanpeisov NU, Nakatsuji H, Hada M, Yoshimoto M (1997) Cluster quantum-chemical MINDO/3 study of HCOOH interactions with nonpolar (100) surface of ZnO. J Mol Catal A 118(1):69–77